



激光加工减反射表面研究进展

矫知真, 李纪超, 陈招弟, 韩冬冬, 张永来*

吉林大学电子科学与工程学院集成光电子学国家重点实验室, 吉林 长春 130012

摘要 材料表面的减反射特性在太阳能的吸收与利用、红外成像、光电子器件和航空航天等领域中具有重要的意义。激光加工作为一种新型、高效、绿色的微纳加工手段在光学领域具有重要的应用价值。激光加工制备的减反射表面在宽光谱、全角度下具有良好的减反特性, 可以有效抑制反射并提高光的透射率/吸收率。详细总结了激光加工减反射表面的最新研究进展, 阐述了减反射原理以及不同需求下减反射材料的选择问题, 探讨了激光加工减反射表面的应用前景, 最后对目前减反射表面存在的局限性和面临的挑战进行了客观讨论, 并对减反射表面的未来发展趋势进行了展望。

关键词 激光技术; 减反射; 激光加工; 微纳结构; 原理

中图分类号 TN249

文献标志码 A

doi: 10.3788/CJL202148.0202011

1 引言

光与物质的相互作用包括吸收、反射、散射、透射、衍射和干涉等^[1]。物质表面的光学特性也就是材料表面对入射电磁波的响应一直备受关注, 增强物质材料对入射光的吸收、透射或反射是研究的重点。物质材料表面的减反射(AR)特性一方面有利于提升特定电磁信号的辨别能力, 另一方面有助于屏蔽与消除特定干扰信号^[2]。降低入射光在物质表面的反射并提高其透射有着至关重要的作用^[3-9]。例如, 在一些光电设备中, 若无法有效地吸收太阳能, 将会造成很大的光能量损失, 进而导致非常低的能量转换效率, 影响器件性能; 在手机和计算机等平板显示中, 眩光的存在会严重影响视觉体验; 透镜、棱镜和平面镜等光学元件中不必要的反射会产生杂散光, 进而影响整体光学系统性能。因此, 进行有效的光管理是至关重要的。

制备减反射表面有很多方式, 包括溶胶凝胶法^[10]、电子束刻蚀^[11]、纳米压印^[12]、湿法刻蚀^[13]和干法刻蚀^[14]等。溶胶凝胶法是一种在温和条件下

制备无机材料的重要方法, 一般用来制备多孔减反射薄膜, 但其制备时间较长。纳米压印利用光刻胶辅助, 将模板上的微纳结构转移到目标材料上, 具有加工简单、快速和精度高等优点, 但涉及到的母模具有制造工艺复杂和成本较高的缺点。湿法刻蚀是一种快速、高效的刻蚀方法, 其将刻蚀材料浸泡在腐蚀溶液内进行腐蚀, 广泛应用于减反射结构的制备, 但这种方法不太容易控制各向同性刻蚀。

激光加工技术解决了上述问题。首先, 激光加工能够满足加工结构的任意性和可控性, 也能够满足加工结构高精度的需求; 其次, 激光加工具有可程序化、适合于大面积加工以及环境友好等优势^[15-21], 并且适用于多种材料的加工, 包括金属、半导体、碳基材料和聚合物等^[22-32], 在微光学元器件和微流控等微纳加工领域得到了广泛研究^[33-38]。除此之外, 激光加工具有结构可设计性, 这有利于减反射结构表面的设计以及后期制备。因此, 激光加工在制备减反射表面领域有着至关重要的作用。

减反射表面广泛应用于工业生产中^[39-41]。例如, 一些博物馆或者展览厅的普通玻璃会造成反光等不

收稿日期: 2020-07-30; 修回日期: 2020-09-08; 录用日期: 2020-09-27

基金项目: 国家重点研发计划(2017YFB1104300)、国家自然科学基金(61935008, 61775078, 61590930)、吉林省科技发展规划(20180101061JC)

*E-mail: yonglaizhang@jlu.edu.cn

良现象,导致展品无法清晰地展示出来,观看体验差,减反射表面可以轻松解决该问题;减反射表面在手机等显示设备上的应用可以使屏幕更加清晰,减小某个波长对眼睛的伤害;在光伏产业中,减反射表面可以有效地提升太阳能电池的光捕获能力,进而提升电池的转换效率。相信有激光加工这把强有力的“刀”作为辅助,减反射表面在工业化中的应用会更丰富。

本文总结了激光加工减反射表面领域的最新研究进展,详细地阐述了减反射原理和减反射材料的选择问题,最后总结了减反射表面在不同领域的应用状况并对其前景进行了展望。

2 基本原理和制备方法

2.1 基本原理

当光线在一种介质中传播时,它的传播路径会保持不变,但是当光线入射到两种折射率不同的介质界面时,光的传播路径就会发生改变,一部分光会返回到原有介质中,这部分就是反射光,这是由边界处的折射率(R)突变引起的。在实际应用中,这部分反射光会造成很大的光能损耗,因此减少材料表面反射光是研究热点。

首先,光由一种介质入射到另一种介质会发生菲涅耳反射,界面处的光反射可以用菲涅耳方程来描述。菲涅耳方程提供了传统的减反射涂层的基本模型^[42],有两个假设:1)反射波具有相同的强度,每个界面反射一个波;2)其他光学的相互作用,如散射和吸收等,可以忽略不计。

基底(折射率为 n_s)上的薄膜(折射率 $n < n_s$)基本遵循薄膜干涉定律,当两个界面处的反射波发生相消干涉时,反射光为零。两个反射波发生相消干涉需满足以下两个条件:1)反射波之间的相位差为 π ;2)薄膜的厚度(d)必须是 $\lambda/4$ 的奇数倍,其中 λ 为入射光光波长。相位差 $\delta = 2\pi nd \cos \theta / \lambda$ (θ 为入射角度),当入射光垂直入射到界面上(即 $\theta=0$)时,界面的反射率 R 可以表达为

$$R = \left(\frac{n_0 n_s - n^2}{n_0 n_s + n^2} \right)^2, \quad (1)$$

式中: n_0 为空气折射率。为了使 $R=0$,由(1)式可知, $n=\sqrt{n_0 n_s}$, $d=\lambda/4n$ 。因此,为了达到最小光反射,调整薄膜的厚度以及折射率是关键。

研究^[43-45]发现,一些夜视昆虫如蛾的复眼表面分布着大量的纳米柱阵列,这种复眼结构使得飞蛾眼表面的反射光几乎不存在,这有利于飞蛾在夜间观察目标,保障了飞蛾的飞行安全。由于其独特的

光学特性,很多研究工作受蛾眼结构启发^[46-48],通过引入微/纳米结构来降低反射率。

下面详细地说明入射光和减反射结构相互作用的机理。

如图1(a)所示,当结构尺寸远大于入射光波长时,部分光被吸收,剩余光被散射和反射;当结构尺寸和入射光波长接近时,如图1(b)所示,光会在结构内部进行多次内反射,形成“光陷”;当结构尺寸是比入射光波长小的纳米结构或亚波长结构时,如图1(c)所示,入射光对这种结构并不敏感且会逐渐弯曲。这是由于这种类似蛾眼结构的纳米结构或亚波长结构等价于具有梯度渐变折射率的减反射层,如图1(d)所示,在入射角改变的情况下,空气和基底之间存在相对平缓的折射率渐变,因此在广角度、宽光谱范围内能够实现低折射率的要求^[49]。

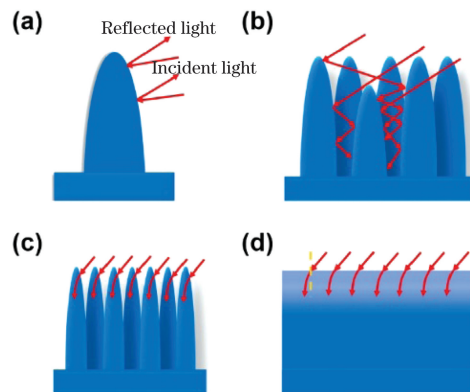


图1 光作用于不同结构尺寸的情况^[50]。(a)光照射到宏观结构单元上;(b)光与微结构作用产生“光陷”; (c)光与纳米结构相互作用;(d)光在折射率呈梯度渐变的表面上逐渐弯曲

Fig. 1 Light acting on structures with different sizes^[50].

- (a) Light irradiating macro-structural unit;
- (b) light interacting with microstructure to form “light trapping”;
- (c) light interacting with nanostructure;
- (d) light gradually bending through surface with refractive index gradient

2.2 制备方法

目前,制备减反射表面的方法通常分为两大类:减反射涂层法和减反射结构。减反射涂层法就是在材料表面引入一层或多层薄膜来达到降低反射率的目的^[51]。从 $n=\sqrt{n_0 n_s}$ 和 $d=\lambda/4n$ 可以看出,一层薄膜对应一个波长,如果需要在多个波长下或者宽波长范围内工作,则需要在材料表面制备几十甚至几百层薄膜来达到减反射的目的。这样的制备方法不仅大大加剧了工艺的复杂性,而且多层薄膜的引入会导致

层与层之间脱落、机械稳定性差及热匹配性较低等,很难满足全角度宽光谱范围内的表面减反射要求。

相比于减反射薄膜,减反射结构具有更高的机械强度以及稳定性,并且表面结构的可设计性强。制备这种减反射结构表面的方法有许多,如化学生长^[52]、等离子体刻蚀^[53]、光刻法^[54]和激光加工等。

化学生长法操作简便,成本低,适用性较好,但存在各向异性刻蚀的问题;等离子体刻蚀法的设备昂贵,成本较高。激光加工是一种十分成熟的加工技术,具有绿色、高效、可设计性强、可大面积加工和无接触等优势。表1详细地展示了各种减反射表面制备方法的优势以及不足之处。

表1 制备减反射表面方法的对比

Table 1 Comparison of methods for fabrication of AR surfaces

Method	AR Structure	Advantage	Disadvantage	Reference
Sol-gel	Double-shelled hollow nanosphere	Simple method and uniform product composition	High cost and consuming time	[10]
Photolithography	Nanoneedle	Facile method, and controllable morphology and size of graphics	Costly and complicated master	[11]
Nano imprinting	Moth's eye nanostructure	High resolution, fast preparation process, and low cost	Costly and complicated master and high environmental standards	[12]
Wet etching	3D compound eye structure	Simple method, fast preparation process, large production area, and good etching selectivity	Poor anisotropy and tough conditions	[13]
Dry etching	Asymmetric nanowire structure	Fast preparation process, high flexibility and anisotropic etching	Expensive equipment	[14]
Chemical vapor growth	Nanocone	Simple device, controllable coating thickness and density	Limited reaction conditions	[51]
Laser processing	Grating structure	Fast preparation process, high efficiency, mass production, green, high precision, and strong controllability	Special equipments	[29]
	Hybrid structure			[55]

激光加工技术目前大致可以分为两种类型:一种为激光直写技术,另一种为激光相干技术。其中,激光直写技术中比较主流的是飞秒激光直写技术,这是因为飞秒激光直写技术具有制备任意复杂二维图形以及三维结构的能力,且具有精度高、热效应小和环境友好等优势。飞秒激光直写技术分为增材制造的双光子聚合技术^[56-60]和减材制造的激光烧蚀加工^[61-63]。其中,飞秒激光烧蚀加工具有逐点扫描加工的特点,这就导致了材料表面长时间曝光或大面积加工时会花费更长时间,影响加工效率。一种提高加工效率的比较有效的方法是多光束并行加工,空间光调制器可以解决以上问题。根据一定的光路设计,通过结合空间光调制器,可以对超快激光的光学参数(相位、振幅或偏振等)进行细致调控,将一个焦点分成多个焦点进行并行加工直写,这样会大大提升加工效率,极大地缩短了加工时间。其次,还有一种比较有效的方法,即先利用飞秒激光在材料表面加工产生表面缺陷,再利用湿法或干法刻蚀进行后续处理,这种以湿法刻蚀或干法刻蚀辅助飞秒激光加工材料的方式能够大大提升加工效率,有

效节省时间,实现高效批量制备。

如果加工大面积的有序周期型结构,激光相干技术^[64]是非常好的加工方式。激光相干系统基于激光全息技术,可制备二维或三维的光子晶体。其原理是多个光束激光的相干叠加,相比于单点加工的激光直写技术,优势是在于可快速、一次成型地加工出大面积微纳米周期结构,大大缩短了加工时间,可实现大批量的制备。

3 材料体系

3.1 硅以及硅的氧化物

硅是光伏产业(如太阳能电池和光电探测器等)最重要的材料之一。因为硅的折射率很大,照射到表面上的光不能够被充分吸收,很大一部分入射光会被反射,硅表面高反射导致的光损耗严重影响了光伏器件的转换效率,所以在硅表面设计结构化的减反射表面是十分必要的^[29,65-66]。研究显示,一维光栅结构可以显著改变半导体表面光学特性,有效地抑制反射光。2011年,Vorobyev等^[29]利用飞秒激光脉冲辐照硅表面,使得硅表面产生周期性纳米

光栅条纹结构。这种结构化的硅表面在紫外到近红外(200~2500 nm)的宽光谱范围内呈现出非常低的反射率,与未处理的硅表面相比,呈现出十分理想的反射效果。

当激光与硅相互作用时,在烧蚀区域周围十分容易产生一些沉积颗粒,这些颗粒和碎屑在加工过程中很容易被氧化成氧化硅而沉积到硅表面,这样制备出的减反射结构表面的性能大打折扣。2020 年,Chen 等^[67]利用激光清洗技术辅助飞秒激光烧蚀硅表面,在一定程度上解决了加工硅需要保护气体的问题。该团队利用激光清洁技术,多次重复地对飞秒激光烧蚀区域进行处理,有效地解决了氧化物沉积的情况。加工产品在 300~2500 nm 范围内的平均反射率为 2.06%。这种制备减反射结构的策略可以用于研究与制备未来光电器件。

二氧化硅(SiO₂)是生活中一种常见且重要的材料,它广泛地应用于玻璃窗户、汽车仪表盘、镜头、眼

镜和光学仪器等光学元件上。在二氧化硅表面制备减反射表面可以有效地防止表面高反射导致的眩光和鬼影等不良现象,从而避免安全隐患以及较差的光学性质等问题。2019 年,Papadopoulos 等^[68]利用圆偏振超短激光脉冲,在熔融石英上诱导出了亚波长纳米柱结构,如图 2(a)所示,纳米柱呈准周期排列形式,但高度和周期是随机的,其中 SEM 表示扫描电镜。从图 2(b)~(d)可以看出,飞秒激光加工二氧化硅比未加工的二氧化硅相比,其透射有一个明显的提升,如果进一步对熔融石英两面进行激光处理,透射会有进一步的提升。此外,在不同入射角情况下,测试了三种不同波长 s 偏振和 p 偏振的入射光的反射和透射光谱,发现即便在大角度入射条件下(>60°),反射率仍小于 5%,即实现了全角度宽光谱范围内的有效减反射结构表面。这种具有超低反射率的透明二氧化硅材料在显示器件和光学元件等领域有着重要的应用前景。

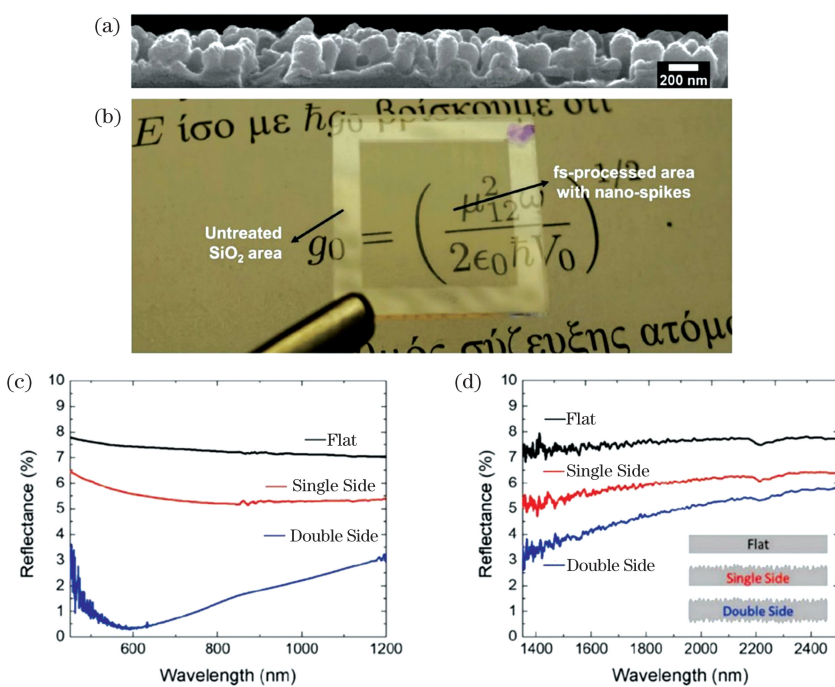


图 2 激光诱导纳米钉的形貌以及反射光谱^[68]。(a)激光诱导形成的纳米钉的横截面 SEM 图;(b)熔融石英样品实物图;(c)未处理样本以及(d)激光处理样本的反射光谱

Fig. 2 Morphology and reflection spectra of laser-induced nanonails^[68]. (a) Cross-sectional SEM image of laser induced nano-nail; (b) picture of fused silica sample; reflectance spectra of (c) untreated and (d) laser-processed samples

3.2 金属

金属材料在很多领域中都有广泛的应用。在金属表面实现减反射特性既可以改善元件表面的光学性质,又为材料的选择提供更多选项^[69]。但是,金属和自由空间之间存在光学阻抗失配,因此在金属表面制备减反射层存在着巨大的挑战。研究表明,

在金属表面引入微纳米结构能够有效地解决这一难题。在微米尺度上,可通过光陷结构来降低反射率。Li 等^[70]利用纳秒激光在钛合金表面进行扫描,制备出的光陷结构表面在 400~1000 nm 处的反射率小于 6%。在纳米尺度上,有序的周期性金属纳米结构可以激发表面等离激元,形成的局域表面等离激

元共振可降低反射。Aydin 等^[71]制备出了超薄(260 nm)Ag-SiO₂-Ag三明治结构,在可见光范围内(400~700 nm)平均光吸收率约为70%,并且这个纳米结构“黑色”超级吸收体对入射光的角度和偏振态不敏感。

具有微纳复合结构的表面可以发挥双重功效,达到有效减反射的目的。2017年,Fan 等^[55]利用脉冲注入控制的激光直写策略,成功地在铜表面制备出了抗反射微纳米混合结构,如图3所示。通过控制激光参数,在多次快速扫描[图3(a)、(c)、(e)]和

单次慢速扫描[图3(b)、(d)、(f)]下进行了多种周期结构的制备,加工出的结构分别为Stru. 1和Stru. 2。如图3(g)所示,在250~2250 nm光谱范围内,结构化的铜表面相较于未结构化的铜,反射率明显降低。在铜、钛和钨表面制备出的这种双尺度结构在紫外到近红外的光谱中分别具有4.1%、2.4%和3.2%的反射率,这在很大程度上推进了金属减反射表面的研究。这种基于金属的减反射结构表面在太阳能的有效吸收和利用及军事隐身等中的应用正进一步展开。

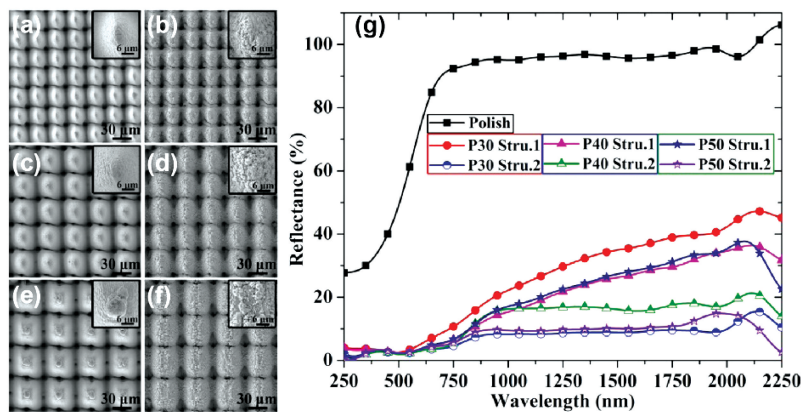


图3 不同结构的SEM图和光谱^[55]。Stru. 1在激光扫描间隔为(a)30 μm,(c)40 μm和(e)50 μm下的SEM图;Stru. 2在激光扫描间隔为(b)30 μm,(d)40 μm,和(f)50 μm下的SEM图;(g)不同激光扫描间隔下两种结构的光谱
Fig. 3 SEM images and spectra of different structures^[55]. SEM images of Stru. 1 under laser scanning intervals of (a) 30 μm, (c) 40 μm and (e) 50 μm; SEM images of Stru. 2 under laser scanning intervals of (b) 30 μm, (d) 40 μm, and (f) 50 μm; (g) spectra of two structures under different laser scanning intervals

虽然这种宏观-微纳结构在紫外到近红外区域具有令人满意的减反射性能,但在中红外等较长波长处的减反射性能却不太令人满意。中红外区域等长波长处的减反射性能面临巨大挑战。Fan 等^[72]利用超快激光预先引入微纳结构,然后利用热氧化法在铜表面生长出高质量的半导体氧化铜纳米线。利用微米结构的“光陷”作用辅助氧化铜纳米线的光学声子耗散,得到的减反射表面在红外波段17 μm左右处的反射率达到极低的0.7%,并在14~18 μm波段达到了超过97%的反射率。这种控制激光直写结合热氧化法的制备策略可以灵活调整减反射结构。

3.3 聚合物

聚合物具有价格低廉、重量轻、柔韧性良好、机械强度高、光学特性优异及适合工业化生产等优势,被广泛应用于生产生活中。研究者已开发出多种基于聚合物的光学增透薄膜,如聚甲基丙烯酸甲酯(PMMA)、聚苯乙烯(PS)、聚对苯二甲酸乙二醇酯(PET)、聚酰亚胺(PI)及聚二甲基硅氧烷(PDMS)等^[73-75]。2014年,Leem 等^[76]利用双光束干涉结合干

法刻蚀和转写技术,在玻璃基底上制备出周期分别为380,500,650 nm的仿反蛾眼结构的PDMS增透层,如图4所示。这种反蛾眼结构相比参考样本PDMS/玻璃,其透射率提高了约2.3%,并且这种结构化表面的疏水性有所提升。这种在宽光谱范围内具有高透射率且具有自清洁性能的减反射层提高了能量转换效率,在有机太阳能电池中发挥了重要的作用。

Wang 等^[77]利用二氧化碳激光雕刻,在PDMS表面一步法制备了微结构,实现了超疏水特性,激光碳化了PDMS表面,使表面吸收率提升至90%左右,为进行有效的光热转换提供了条件,并且利用激光直写将其设计成不同的形状,如齿轮和鱼等,制备出了光驱动浮动器件。这种方法为光驱动制动器提供了一种高效、低成本、简单的方法,同时也为各种类型的驱动器表面结构的设计与制备提供了思路^[78-84]。除此之外,Müller-Meskamp 等^[85]利用高功率脉冲激光器,在PET薄膜上进行直接激光干涉图案化处理,将周期性光栅引入薄膜表面,该结构化PET薄膜的吸收率在300~800 nm区间有了显著

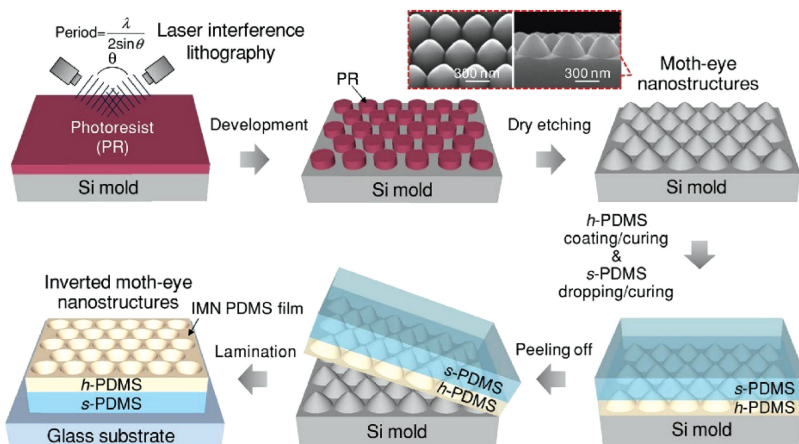


图4 在Si模板上利用激光干涉和PDMS转写技术制备反蛾眼纳米阵列结构的流程^[76]

Fig. 4 Flow chart for preparing anti-moth-eye nanoarray structure on Si template using laser interference and PDMS transfer technology^[76]

的提升,这有助于提升有机太阳能电池器件的性能。

3.4 其他材料

在红外波段,普通硅基玻璃很难实现优异的光学性能。红外材料主要由硫化物和卤化物构成,而硫化物具备很好的光学性能,在红外波段具有较好的光学特性。因此,ZnS作为重要的二六族化合物半导体在红外窗口是很理想的基底材料,受到了极大的关注,在光电器件等领域有着广泛的应用。ZnS材料不仅带隙宽、折射率高,而且在可见光范围内具有很高的透射率,有着巨大的应用潜力。2011年,Wang等^[86]利用激光干涉直接在ZnS基板上进行烧蚀,通过调节和控制脉冲数来调节表面柱状形态,在垂直入射时实现了红外波长的高透过率(>92%)。

蓝宝石具有良好的光学透明度、较宽的工作波段及较好的化学性能和机械稳定性等,被广泛地用于机载光电设备和红外探测设备等方面。蓝宝石作

为优秀的透波材料,在紫外到红外波段均具有良好透率。Li等^[87]利用飞秒激光直写结合湿法腐蚀,在蓝宝石上制备了周期约为2 μm、高度约为900 nm的倒金字塔和圆锥阵列型中红外亚波长纳米结构,该结构在3~5 μm范围内展现出了高透射率并具有角度不依赖特性。

石墨烯材料是一种具有代表性的二维碳纳米材料。由于其π键具有很好的光学性能,石墨烯材料在光存储、光电探测及传感等诸多领域显示出巨大的应用价值。Zhang等^[88]利用激光诱导还原冻干的石墨烯氧化物,制备出由石墨烯组装的垂直有序的柱阵列框架(HOPGF),其吸收率在湿润的条件下可以达到98%。将HOPGF作为光吸收层,20 min内表面温度就从20 °C升到40 °C左右。表2直观地展示了激光加工制备的各种减反射材料的反射率、透射率、吸收率以及对应波长。

表2 激光加工制备的各种减反射材料的反射率、透射率、吸收率以及波长

Table 2 Reflectivity, transmissivity, absorptivity and wavelength of each AR material prepared by laser processing

Material	Reflectivity /%	Transmissivity /%	Absorptivity /%	Wavelength	Reference
Si	About 3.5	—	—	250~2500 nm	[29]
	2.06	—	—	300~2500 nm	[67]
SiO ₂	<4	—	—	450~1200 nm	[68]
Ti alloy	<6	—	—	500~1000 nm	[70]
Ag-SiO ₂ -Ag	—	—	70	400~700 nm	[71]
Cu	<5	—	—	250~2250 nm	[55]
	<3	—	—	14~18 μm	[72]
PDMS	—	>94.2	—	350~800 nm	[76]
	—	—	90	240~1050 nm	[77]
ZnS	—	>92	—	8~10 μm	[86]
Sapphire	—	>85	—	3~5 μm	[87]
Graphene	—	—	98	250~2500 nm	[88]

4 应用

4.1 太阳能电池

随着人类社会的不断发展,能源问题成为制约社会发展的主要问题。人们对可再生能源的需求日益增加,促使光伏产业日益蓬勃。对于太阳能电池来说,有效地进行光捕获是至关重要的,因此制备减反射表面对于提高太阳能电池的功率转换效率(PCE)有着重要的作用^[89-93]。减反射结构的引入可以十分显著地改善光吸收,提供全角度宽光谱范围内的低反射率,使得结构表面具有自清洁功能,这些均能够改善器件在实际应用中的性能。

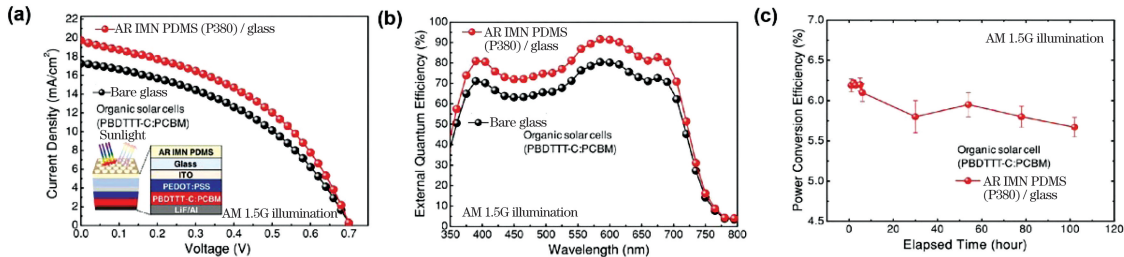


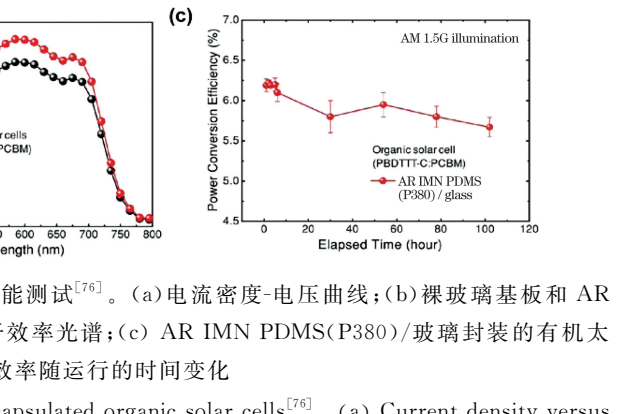
图 5 AR IMN PDMS(P380)/玻璃封装的有机太阳能电池的性能测试^[76]。(a) 电流密度-电压曲线;(b) 裸玻璃基板和 AR IMN PDMS(P380)/玻璃封装的有机太阳能电池的外量子效率光谱;(c) AR IMN PDMS(P380)/玻璃封装的有机太阳能电池的能量转换效率随运行的时间变化

Fig. 5 Performance tests of AR IMN PDMS (P380)/glass encapsulated organic solar cells^[76]. (a) Current density versus voltage; (b) external quantum efficiency spectra of bare glass substrate and AR IMN PDMS (P380) / glass encapsulated organic solar cells; (c) power conversion efficiency of AR IMN PDMS (P380) / glass encapsulated organic solar cells versus operation time

4.2 发光二极管/有机发光二极管

发光二极管(LED)和有机发光二极管(OLED)作为显示照明设备,在生产生活中得到了广泛的应用。其中,光提取效率对器件来说是十分重要的,但由于空气和器件基底存在折射率失配,当光子出射到空气中时会产生菲涅耳反射和全反射,大部分的光子会折回到器件内部直至被吸收,这严重影响了光提取效率^[94]。为了解决这一问题,在器件上通过引入微纳米双尺度复合结构来减少反射,进而增大外量子提取效率^[95]。Bi 等^[96]将双周期波纹结构引入到金属电极上,如图 6(a)所示。图 6(b)~(d)分别为光栅周期为 225 nm 和 325 nm 的波纹结构(1D)及组合后双周期的波纹结构(2D),其中 AFM 表示原子力显微镜。图 6(e)、(f)对比了双周期波纹结构和一维单周期波纹结构以及平面的白光 OLED 的电致发光性能,可以发现,双周期波纹结构的引入对 OLED 的最大亮度以及最大电流效率有着很大的提升作用。测试表明,双周期波纹结构器件相比于平

面器件,最大亮度提升了 18960 cd/m⁻² 左右[图 6(e)],最大电流效率提升了 6.06 cd/A[图 6(f)]。Leem 等^[76]利用双光束干涉结合干法刻蚀和转写技术,在玻璃基底上制备出具有仿反蛾眼结构的 PDMS 增透层(AR IMN PDMS),如图 4 所示。这种反蛾眼结构的透射率相比原本 PDMS/玻璃提高了约 2.3%。如图 5(a)、(b)所示,其中表面周期为 380 nm 的整个器件[AR IMN PDMS(P380)]相比玻璃基板,电流密度以及外量子效率有了较好的提升。这是由于空气与 PDMS 之间存在呈连续线性梯度变化的折射率,因此这种周期小于入射光波长的反蛾眼结构可以有效地减少反射光。并且在长达 100 h 的测试中,整体器件的能量转换效率能够保持相对稳定的状态,如图 5(c)所示。



面器件,最大亮度提升了 18960 cd/m⁻² 左右[图 6(e)],最大电流效率提升了 6.06 cd/A[图 6(f)]。

Liu 等^[5]先利用 266 nm 紫外激光器对硅基底上的光刻胶进行图案化处理,后利用转写技术制备出具有波纹状纳米结构的有机发光器件,通过对空穴传输层进行图案化处理来增强光提取效率。与平面器件相比,最大亮度和电流效率分别提高了 24% 和 20%。

目前已有很多工作致力于提高光提取效率,但是要实现基于减反结构的 LED/OLED 的广泛应用,我们应该着重研究减反射材料的合理选择、减反结构的理论优化与设计以及制备工艺之间的有机结合。

4.3 光电探测器

除了太阳能电池和 LED/OLED 之外,减反射结构表面也广泛应用于光电探测器中。光电探测器能够把光信号转换为电信号,其原理是半导体材料的光电导效应,即利用光照辐射改变被辐照材料表面的电导率。光电探测器在红外成像和红外遥感等

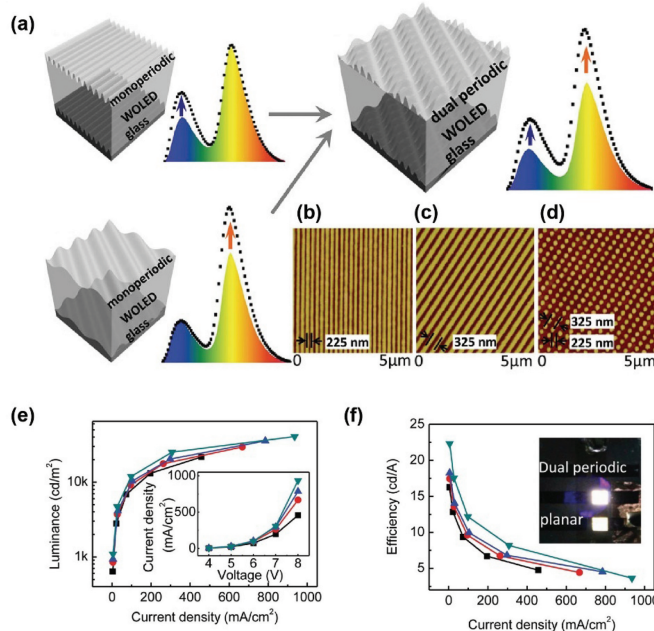


图 6 双周期波纹结构的形貌以及性能^[96]。(a)双周期波纹结构用于宽带光提取的示意图;(b)~(d)一维单周期波纹结构以及双周期波纹结构的表面 AFM 图;(e)电流密度-亮度曲线(插图为电流密度-电压曲线);(f)电流密度-效率曲线(插图为相同驱动电压下运行的双周期和平板 OLED)

Fig. 6 Morphology and performance of double-periodic corrugated structure^[96]. (a) Schematic of double-periodic corrugated structure used for broadband light extraction; (b)–(d) surface AFM images of 1D single- and double-periodic corrugated structure ; (e) current density versus brightness (current density versus voltage characteristics shown in inset); (f) current density versus efficiency (double-periodic and planar OLEDs operating at same driving voltage)

领域有着至关重要的作用。减反射结构可以增加器件的光吸收,对提高光电探测器的灵敏度有很大帮助。Li 等^[97]在氮气下利用飞秒激光辐照硅表面,同时将 N 原子掺杂到结构化的硅表面,最后制备了单吸收层的光电探测器[如图 7(a)所示]和双吸收层的光电探测器[如图 7(b)所示]。这两种器件的电流-电压(I-V)曲线分别如图 7(c)、(d)所示。通过测试发现,相比单吸收层,双吸收层在相同的反向偏压下将光响应性提高至 5.3 mA/W,如图 7(f)所示。

Li 等^[98]在氩气气氛中的近本征硅衬底上利用纳秒激光制造了非掺杂黑硅,这些样品在 1100~2500 nm 范围内的吸收率大于 50%,均表现出高吸收率,并制备出了基于非掺杂黑硅材料的红外光电二极管。在 10 V 反向偏压下,光电二极管在 1310 nm 处的响应度高达 256 mA/W。

光电探测器正向高速、高灵敏度和宽带宽的方向飞速发展,其可广泛应用于光通信系统、信号处理装置以及传感装置等复杂系统中,相信以激光加工技术进行辅助,具有宽带、全角度以及高吸收等减反射性能的表面将赋予光电探测器更灵敏的特性。

4.4 太阳能驱动水蒸发

除了光电转换,光热转换也是非常重要的能量

转化形式,其可有效地进行光捕获,这对于能源的利用和发展是有重要意义的^[99-100]。

太阳能是非常重要的可再生能源,有效地收集并利用太阳能进行光热转换以驱动海水淡化是目前解决淡水资源短缺的一个重要途径^[101-104]。其中,制备具有高光吸收率和高光热转换效率的光热层是十分重要的,这影响着海水淡化的速率和整体器件的性能。He 等^[105]利用纳秒激光系统,在铜表面制备出的减反结构在 220~800 nm 和 220~2500 nm 范围内的反射率分别低于 1.1% 和 8.1%,在 15 个太阳光照下光热效率超过 52%。2016 年,Fan 等^[106]利用飞秒激光直写在铜表面制备出花椰菜结构,其在 200~800 nm 范围内的吸收率高达 98%,并将其用作光热转换层[如图 8(a)所示],在 1 kW·h⁻¹ 太阳光照射下,整体光热转换效率提升到 60%以上[图 8(b)]。飞秒激光制备的基于微纳米结构的光热层在很大程度上提高了水蒸发效率,步骤简单,适合大面积加工,有利于解决能源效率问题。

4.5 仿生多功能表面

在实际应用场景中,这些具有减反射表面的器

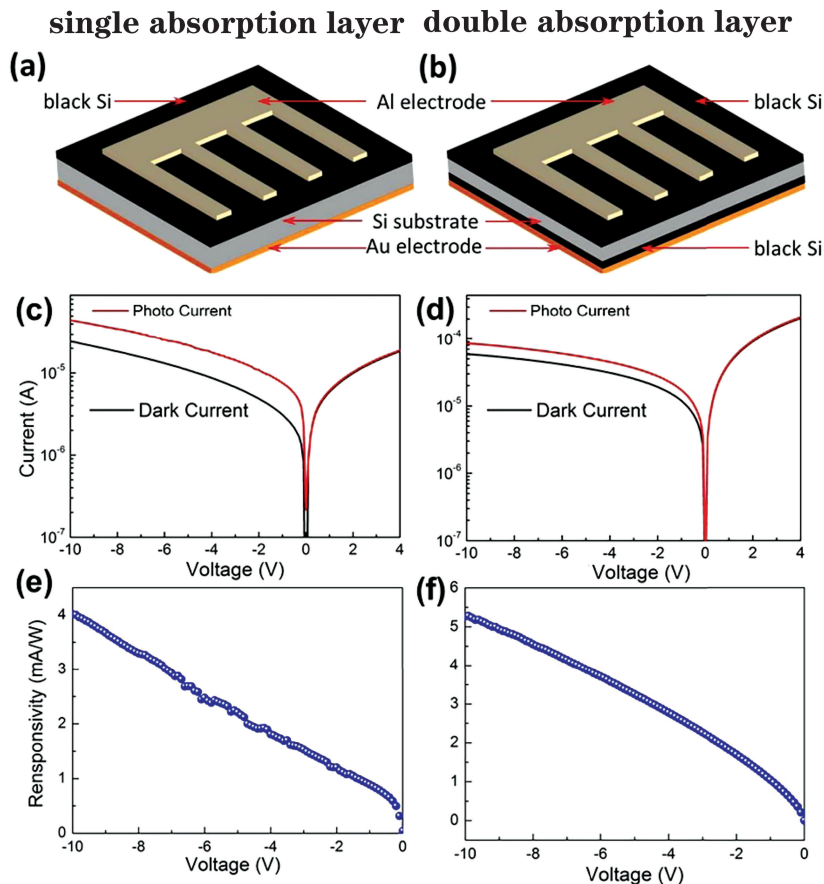


图 7 氮掺杂的单/双吸收层光电探测器性能对比^[97]。(a)(b)两个不同氮掺杂光电探测器的示意图;(c)(d)电流与电压的关系;(e)(f)响应度与电压的关系

Fig. 7 Performance comparison of nitrogen-doped single/double absorption layer photodetectors^[97].(a)(b) Schematic of two different nitrogen-doped photodetectors; (c)(d) relationship between photocurrent and dark current ; (e)(f) relationship between responsivity and voltage

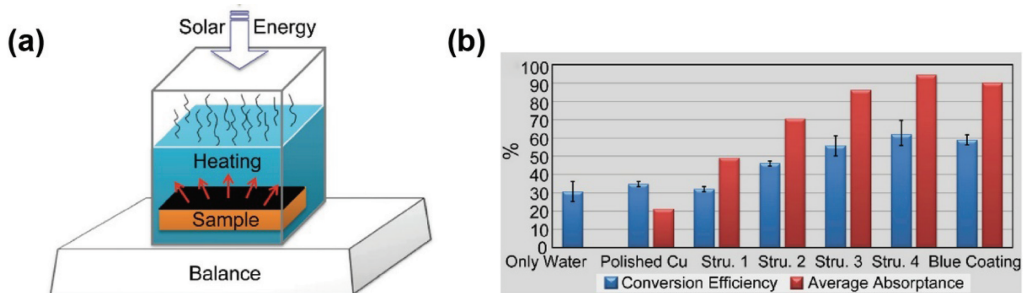


图 8 太阳能驱动界面蒸发表示意图以及性能对比^[106]。(a)太阳能驱动水蒸发装置示意图;(b)1个太阳光下不同样品的光热转换效率与平均吸收率

Fig. 8 Schematic diagram of solar-driven interface evaporation and performance comparison^[106].(a) Schematic of solar-driven water evaporation device; (b) light-to-heat conversion efficiency and average absorption rate of each sample under one sunlight

件会不可避免地遇到极端条件,如雾天、雨天、多尘环境和多菌环境等。这就要求减反射表面在保持自身原有减反特性的同时具备其他功能,如自清洁、防水雾、抗结冰、抗菌^[54] 和防腐蚀^[107] 等。Lian 等利用纳秒激光在钛合金表面加工了周期为 5~

$60 \mu\text{m}$ 条纹并进行了低温退火处理。这种表面具有低于 10% 的反射率,在空气中呈现超疏水特性,在水中具有超亲油特性;利用乙醇进行预润湿后,在水下呈现超疏油特性,其中超亲/疏油特性可不断重复。这种减反射表面的水下超亲/疏油特性在气泡

或油滴的操控方面有很好的前景^[109-112]。

具有超疏水特性的材料表面在自清洁过程中有一个非常重要的作用,水滴会带走堆积在表面的灰尘等污染物,从而实现自清洁^[113]。在外部环境中放置太久的太阳能电池的表面会积灰,这会严重影响太阳光的吸收效率,进而影响器件性能。因此,具有自清洁功能的减反射表面是十分必要的。Mao等^[114]先用离子束溅射二氧化硅薄膜的铜基底,利用800 nm激光在表面加工点阵结构,之后在450 ℃下退火生长CuO纳米线。加工后的表面在600~1150 nm光谱范围内的反射率高于94%,且疏水角约为160°,滑动角小于1.7°。这展现了减反射表面优异的自清洁特性。Domke等^[115]利用超短脉冲激光制备了基于玻璃的防水雾表面,其可应用于建筑结构中的窗户、汽车车窗以及医护人员的医疗眼镜上。霜冻是一种常见的自然气象,由于温度的骤降,物体或植物表面会结霜,这会对日常出行交通、建筑物、高压电缆和农作物经济等产生巨大的负面影响。因此高效、无害的抗霜冻表面是急迫需要的。Li等^[116]利用1060 nm激光在铜表面进行点阵和周期性条纹的加工,对比测试发现,加工后的表面能够大大延长结冰时间。

以上例子说明减反射表面在一定情况下需要进行多功能集成,进而实现多元化的应用。

5 结束语

基于微纳结构的减反射表面具有广角度、宽光谱以及偏振不敏感等优异特性,在太阳能电池、LED、OLED、光电探测器以及光热转换等方面得到了广泛的应用。从减反射表面原理、减反材料的选择以及应用方面,对减反射表面进行了介绍,对近年来国内外的研究进展进行了总结。

目前,激光加工减反射表面虽然取得了一定的进步,但是仍存在一些亟待解决的问题。1)尽管激光加工技术是一种先进的微纳加工手段,但也存在局限性,如加工效率低等,所以可以将激光加工与其他制备工艺进行结合,为设计和制备减反射表面提供更多的选择。2)材料表面的减反射性质蕴含了自然界生物表面结构的密码,通过激光加工进行减反射表面的制备一直是研究热点。目前减反射表面的微结构种类形貌(金字塔、纳米钉、光栅等)有一定的局限性,从自然界生物表面结构获取灵感并将其应用于表面工程科学是巨大的挑战;现有的减反射表面大多局限在平面上,结合实际需求,可以将其应用

于曲面,这样制备的减反射表面的应用范围会更加广泛。针对这些挑战,首先应该从减反射结构的设计与优化入手,同时继续探索自然界生物表面,在此基础上将平面上的二维结构扩展到三维以满足更多需求。3)一些用在太阳能电池和OLED等上的减反射表面不可避免地会在恶劣条件下使用,减反射表面在保持表面减反射特性的同时还需具有机械稳定性、热稳定性和化学稳定性等。为解决此问题,针对不同的需求选择合适的减反材料以及加工方法,并开发多种功能的集成化的减反射表面。

尽管激光加工制备减反射表面还存在一些问题,但是通过深入研究减反射表面理论,优化减反射表面结构,并结合其他制备工艺,一定会制备出更加优异的集成化减反射表面。这将提升发光器件等的性能,进而推动能源领域的发展。

参 考 文 献

- [1] Tadepalli S, Slocik J M, Gupta M K, et al. Bio-optics and bio-inspired optical materials[J]. Chemical Reviews, 2017, 117(20): 12705-12763.
- [2] Fan P X, Zhong M L. Progress on ultrafast laser fabricating metal surface micro-nano antireflection structures[J]. Infrared and Laser Engineering, 2016, 45(6): 0621001.
- [3] Jin Y, Feng J, Zhang X L, et al. Solving efficiency-stability tradeoff in top-emitting organic light-emitting devices by employing periodically corrugated metallic cathode[J]. Advanced Materials, 2012, 24(9): 1187-1191.
- [4] Li C H, Zhao J H, Yu X Y, et al. Fabrication of black silicon with thermostable infrared absorption by femtosecond laser [J]. IEEE Photonics Journal, 2016, 8(6): 1-9.
- [5] Liu Y F, An M H, Zhang X L, et al. Enhanced efficiency of organic light-emitting devices with corrugated nanostructures based on soft nano-imprinting lithography[J]. Applied Physics Letters, 2016, 109(19): 193301.
- [6] Han D D, Chen Z D, Li J C, et al. Airflow enhanced solar evaporation based on Janus graphene membranes with stable interfacial floatability [J]. ACS Applied Materials & Interfaces, 2020, 12(22): 25435-25443.
- [7] Tan G, Lee J H, Lan Y H, et al. Broadband antireflection film with moth-eye-like structure for flexible display applications[J]. Optica, 2017, 4(7):

- 678-683.
- [8] Moghimi M J, Lin G Y, Jiang H R. Broadband and ultrathin infrared stealth sheets [J]. Advanced Engineering Materials, 2018, 20(11): 1800038.
- [9] Daglar B, Khudiyev T, Demirel G B, et al. Soft biomimetic tapered nanostructures for large-area antireflective surfaces and SERS sensing [J]. Journal of Materials Chemistry C, 2013, 1(47): 7842-7848.
- [10] Yao L, He J H, Geng Z, et al. Fabrication of mechanically robust, self-cleaning and optically high-performance hybrid thin films by SiO_2 & TiO_2 double-shelled hollow nanospheres [J]. Nanoscale, 2015, 7(30): 13125-13134.
- [11] Kim D S, Jeong Y, Jeong H, et al. Triple-junction InGaP/GaAs/Ge solar cells integrated with polymethyl methacrylate subwavelength structure [J]. Applied Surface Science, 2014, 320: 901-907.
- [12] Raut H K, Dinachali S S, He A Y, et al. Robust and durable polyhedral oligomeric silsesquioxane-based anti-reflective nanostructures with broadband quasi-omnidirectional properties [J]. Energy & Environmental Science, 2013, 6(6): 1929.
- [13] Shi G, Guo J L, Wang L K, et al. Photoactive PANI/ TiO_2 /Si composite coatings with 3D bio-inspired structures [J]. New Journal of Chemistry, 2017, 41(15): 6965-6968.
- [14] Ko M D, Rim T, Kim K, et al. High efficiency silicon solar cell based on asymmetric nanowire [J]. Scientific Reports, 2015, 5: 11646.
- [15] Zhang Y L, Chen Q D, Xia H, et al. Designable 3D nanofabrication by femtosecond laser direct writing [J]. Nano Today, 2010, 5(5): 435-448.
- [16] Zhang Y L, Guo L, Wei S, et al. Direct imprinting of microcircuits on graphene oxides film by femtosecond laser reduction [J]. Nano Today, 2010, 5(1): 15-20.
- [17] Kawata S, Sun H B, Tanaka T, et al. Finer features for functional microdevices [J]. Nature, 2001, 412 (6848): 697-698.
- [18] Zhang Y L, Tian Y, Wang H, et al. Dual-3D femtosecond laser nanofabrication enables dynamic actuation [J]. ACS Nano, 2019, 13(4): 4041-4048.
- [19] Fang H H, Yang J, Ding R, et al. Polarization dependent two-photon properties in an organic crystal [J]. Applied Physics Letters, 2010, 97 (10): 101101.
- [20] Liu Y Q, Mao J W, Chen Z D, et al. Three-dimensional micropatterning of graphene by femtosecond laser direct writing technology [J]. Optics Letters, 2020, 45(1): 113-116.
- [21] Wu D, Wu S Z, Niu L G, et al. High numerical aperture microlens arrays of close packing [J]. Applied Physics Letters, 2010, 97(3): 031109.
- [22] Lapointe J, Bérubé J P, Ledemi Y, et al. Nonlinear increase, invisibility, and sign inversion of a localized fs-laser-induced refractive index change in crystals and glasses [J]. Light: Science & Applications, 2020, 9: 64.
- [23] You R, Liu Y Q, Hao Y L, et al. Laser fabrication of graphene-based flexible electronics [J]. Advanced Materials, 2020, 32(15): e1901981.
- [24] You R, Han D D, Liu F M, et al. Fabrication of flexible room-temperature NO_2 sensors by direct laser writing of In_2O_3 and graphene oxide composites [J]. Sensors and Actuators B: Chemical, 2018, 277: 114-120.
- [25] Jiang H B, Liu Y, Liu J, et al. Moisture-responsive graphene actuators prepared by two-beam laser interference of graphene oxide paper [J]. Frontiers in Chemistry, 2019, 7: 464.
- [26] Zhang D S, Ranjan B, Tanaka T, et al. Carbonized hybrid micro/nanostructured metasurfaces produced by femtosecond laser ablation in organic solvents for biomimetic antireflective surfaces [J]. ACS Applied Nano Materials, 2020, 3(2): 1855-1871.
- [27] Roberts A S, Novikov S M, Yang Y Q, et al. Laser writing of bright colors on near-percolation plasmonic reflector arrays [J]. ACS Nano, 2019, 13(1): 71-77.
- [28] AlQattan B, Yetisen A K, Butt H. Direct laser writing of nanophotonic structures on contact lenses [J]. ACS Nano, 2018, 12(6): 5130-5140.
- [29] Vorobyev A Y, Guo C L. Antireflection effect of femtosecond laser-induced periodic surface structures on silicon [J]. Optics Express, 2011, 19(Suppl 5): A1031-A1036.
- [30] Guo T Y, Zhang L M, Ren Y Y, et al. Surface characteristics of CaF_2 crystal ablated by femtosecond laser [J]. Acta Optica Sinica, 2019, 39(1): 0126019. 郭太勇, 张立木, 任莹莹, 等. 飞秒激光烧蚀氟化钙晶体表面特性 [J]. 光学学报, 2019, 39 (1): 0126019.
- [31] Han D D, Cai Q, Li J C, et al. Preparation of laser induced graphene based underwater superoleophobic bionic surface [J]. Laser & Optoelectronics Progress, 2020, 57(15): 151408. 韩冬冬, 蔡青, 李纪超, 等. 激光诱导石墨烯水下超疏油仿生表面的制备 [J]. 激光与光电子学进展, 2020, 57(15): 151408.
- [32] Wu X F, Yin H L, Li Q. Femtosecond laser processing of carbon nanotubes film [J]. Chinese Journal of Lasers, 2019, 46(9): 0902002. 吴雪峰, 尹海亮, 李强. 飞秒激光加工碳纳米管薄膜

- 试验研究[J]. 中国激光, 2019, 46(9): 0902002.
- [33] Fu X Y, Chen Z D, Han D D, et al. Laser fabrication of graphene-based supercapacitors [J]. Photonics Research, 2020, 8(4): 577-588.
- [34] Liu Y Q, Chen Z D, Mao J W, et al. Laser fabrication of graphene-based electronic skin [J]. Frontiers in Chemistry, 2019, 7: 461.
- [35] Wu D, Chen Q D, Niu L G, et al. Femtosecond laser rapid prototyping of nanoshells and suspending components towards microfluidic devices[J]. Lab on a Chip, 2009, 9(16): 2391-2394.
- [36] Fang H H, Ding R, Lu S Y, et al. Distributed feedback lasers based on thiophene/phenylene co-oligomer single crystals [J]. Advanced Functional Materials, 2012, 22(1): 33-38.
- [37] Zou T T, Zhao B, Xin W, et al. High-speed femtosecond laser plasmonic lithography and reduction of graphene oxide for anisotropic photoresponse [J]. Light: Science & Applications, 2020, 9: 69.
- [38] Sakakura M, Lei Y H, Wang L, et al. Ultralow-loss geometric phase and polarization shaping by ultrafast laser writing in silica glass[J]. Light: Science & Applications, 2020, 9: 15.
- [39] Liu Z H. Development status and trend of antireflective glass in China[J]. Glass, 2019, 46(8): 1-8.
刘志海. 我国减反射玻璃发展现状及趋势[J]. 玻璃, 2019, 46(8): 1-8.
- [40] Kong W J, Cao K H, You C L, et al. Optimization of wide spectrum anti-reflective grating for solar cell [J]. Acta Optica Sinica, 2013, 33(12): 1205001.
孔伟金, 曹凯华, 由成龙, 等. 太阳能电池用宽光谱减反射光栅的优化设计[J]. 光学学报, 2013, 33(12): 1205001.
- [41] Lin S H, Zhang J, Ai L, et al. Advances in antireflection coatings on photovoltaic glass [J]. Materials Review, 2019, 33(21): 3588-3595.
林昇华, 张景, 艾玲, 等. 光伏玻璃减反射膜的研究进展[J]. 材料导报, 2019, 33(21): 3588-3595.
- [42] Raut H K, Ganesh V A, Nair A S, et al. Anti-reflective coatings: a critical, in-depth review [J]. Energy & Environmental Science, 2011, 4 (10): 3779.
- [43] Clapham P B, Hutley M C. Reduction of lens reflexion by the "moth eye" principle [J]. Nature, 1973, 244(5414): 281-282.
- [44] Brunner R, Sandfuchs O, Pacholski C, et al. Lessons from nature: biomimetic subwavelength structures for high-performance optics [J]. Laser & Photonics Reviews, 2012, 6(5): 641-659.
- [45] Wilson S J, Hutley M C. The optical properties of 'moth eye' antireflection surfaces[J]. Optica Acta: International Journal of Optics, 1982, 29 (7): 993-1009.
- [46] Lin H, Fu Y G, Ouyang M Z, et al. Design and analysis of moth-eye antireflective metasurface structure with broadband and wide-angle[J]. Chinese Journal of Lasers, 2019, 46(1): 0113002.
林鹤, 付跃刚, 欧阳名钊, 等. 宽光谱广角蛾眼抗反射超表面结构设计分析[J]. 中国激光, 2019, 46(1): 0113002.
- [47] Ghymn Y H, Jung K, Shin M, et al. A luminescent down-shifting and moth-eyed anti-reflective film for highly efficient photovoltaic devices [J]. Nanoscale, 2015, 7(44): 18642-18650.
- [48] Ji S, Park J, Lim H. Improved antireflection properties of moth eye mimicking nanopillars on transparent glass: flat antireflection and color tuning [J]. Nanoscale, 2012, 4(15): 4603-4610.
- [49] Rayleigh L. On reflection of vibrations at the confines of two media between which the transition is gradual [J]. Proceedings of the London Mathematical Society, 1879, s-11(1): 51-56.
- [50] Han Z W, Jiao Z B, Niu S C, et al. Ascendant bioinspired antireflective materials: opportunities and challenges coexist[J]. Progress in Materials Science, 2019, 103: 1-68.
- [51] Corrigan T D, Park D H, Drew H D, et al. Broadband and mid-infrared absorber based on dielectric-thin metal film multilayers [J]. Applied Optics, 2012, 51(8): 1109-1114.
- [52] Park K C, Choi H J, Chang C H, et al. Nanotextured silica surfaces with robust superhydrophobicity and omnidirectional broadband supertransmissivity [J]. ACS Nano, 2012, 6 (5): 3789-3799.
- [53] Kumar A, Yerva S V, Barshilia H C. Broadband and wide angle anti-reflective nanoporous surface on poly (ethylene terephthalate) substrate using a single step plasma etching for applications in flexible electronics [J]. Solar Energy Materials and Solar Cells, 2016, 155: 184-193.
- [54] Kim S, Jung U T, Kim S K, et al. Nanostructured multifunctional surface with antireflective and antimicrobial characteristics [J]. ACS Applied Materials & Interfaces, 2015, 7(1): 326-331.
- [55] Fan P X, Bai B F, Zhong M L, et al. General strategy toward dual-scale-controlled metallic micro-nano hybrid structures with ultralow reflectance[J]. ACS Nano, 2017, 11(7): 7401-7408.
- [56] Sun H B, Kawata S. Two-photon

- photopolymerization and 3D lithographic microfabrication [M]//NMR 3D analysis photopolymerization. Advances in polymer science. Heidelberg: Springer, 2006, 170: 169-273.
- [57] Xing J F, Zheng M L, Duan X M. Two-photon polymerization microfabrication of hydrogels: an advanced 3D printing technology for tissue engineering and drug delivery [J]. Chemical Society Reviews, 2015, 44(15): 5031-5039.
- [58] Carlotti M, Mattoli V. Functional materials for two-photon polymerization in microfabrication [J]. Small, 2019, 15(40): 1902687.
- [59] Sun R, Wang Z Y, Hu Y L, et al. Processing and application of hydrogel Janus micropillars based on femtosecond laser [J]. Chinese Journal of Lasers, 2019, 46(9): 0902001.
孙锐, 王重宇, 胡衍雷, 等. 飞秒激光加工水凝胶双面神微柱及其应用 [J]. 中国激光, 2019, 46(9): 0902001.
- [60] Qiao L L, Chu W, Wang Z, et al. Three-dimensional microfabrication by shaped femtosecond laser pulses [J]. Acta Optica Sinica, 2019, 39(1): 0126012.
乔玲玲, 储蔚, 王哲, 等. 基于整形飞秒激光脉冲的三维微纳制备 [J]. 光学学报, 2019, 39(1): 0126012.
- [61] Li Y, Itoh K, Watanabe W, et al. Three-dimensional hole drilling of silica glass from the rear surface with femtosecond laser pulses [J]. Optics Letters, 2001, 26(23): 1912-1914.
- [62] Bonse J, Höhm S, Kirner S V, et al. Laser-induced periodic surface structures: a scientific evergreen [J]. IEEE Journal of Selected Topics in Quantum Electronics, 2017, 23(3): 16516265.
- [63] Ahmmed K, Grambow C, Kietzig A M. Fabrication of micro/nano structures on metals by femtosecond laser micromachining [J]. Micromachines, 2014, 5(4): 1219-1253.
- [64] Jiang H B, Zhang Y L, Han D D, et al. Bioinspired fabrication of superhydrophobic graphene films by two-beam laser interference [J]. Advanced Functional Materials, 2014, 24(29): 4595-4602.
- [65] Yang J, Luo F F, Kao T S, et al. Design and fabrication of broadband ultralow reflectivity black Si surfaces by laser micro/nanoprocessing [J]. Light: Science & Applications, 2014, 3(7): e185.
- [66] Lü X Z, Ji L F, Wu Y, et al. Fabrication of high performance anti-reflection silicon surface by picosecond laser scanning irradiation with chemical corrosion [J]. Chinese Journal of Lasers, 2015, 42(4): 0403006.
吕晓占, 季凌飞, 吴燕, 等. 皮秒激光-化学复合法制备高效减反射晶硅表面微结构研究 [J]. 中国激光, 2015, 42(4): 0403006.
- [67] Chen T, Wang W J, Tao T, et al. Multi-scale micro-nano structures prepared by laser cleaning assisted laser ablation for broadband ultralow reflectivity silicon surfaces in ambient air [J]. Applied Surface Science, 2020, 509: 145182.
- [68] Papadopoulos A, Skoulas E, Mimidis A, et al. Biomimetic omnidirectional antireflective glass via direct ultrafast laser nanostructuring [J]. Advanced Materials, 2019, 31(32): e1901123.
- [69] Qin X Y, Huang T, Xiao R S. Periodic microstructure on Ti surface induced by high-power green femtosecond laser [J]. Chinese Journal of Lasers, 2019, 46(10): 1002006.
秦晓阳, 黄婷, 肖荣诗. 高功率绿光飞秒激光诱导产生钛表面周期性微结构 [J]. 中国激光, 2019, 46(10): 1002006.
- [70] Li J R, Xu J K, Lian Z X, et al. Fabrication of antireflection surfaces with superhydrophobic property for titanium alloy by nanosecond laser irradiation [J]. Optics & Laser Technology, 2020, 126: 106129.
- [71] Aydin K, Ferry V E, Briggs R M, et al. Broadband polarization-independent resonant light absorption using ultrathin plasmonic super absorbers [J]. Nature Communications, 2011, 2: 517.
- [72] Fan P X, Bai B F, Long J Y, et al. Broadband high-performance infrared antireflection nanowires facilely grown on ultrafast laser structured Cu surface [J]. Nano Letters, 2015, 15(9): 5988-5994.
- [73] Chen S F, Chen B L, Huang C Q, et al. An antireflection method for a fluorinated ethylene propylene (FEP) film as short pulse laser debris shields [J]. RSC Advances, 2016, 6(92): 89387-89390.
- [74] Kok S Y, Tou T Y, Yap S L, et al. Pulsed laser interference patterning of polyimide grating for dye-doped polymer laser [J]. Journal of Nanophotonics, 2016, 10(3): 033003.
- [75] Rodriguez-Rodriguez Á, Rebollar E, Soccio M, et al. Laser-induced periodic surface structures on conjugated polymers: poly (3-hexylthiophene) [J]. Macromolecules, 2015, 48(12): 4024-4031.
- [76] Leem J W, Kim S, Lee S H, et al. Efficiency enhancement of organic solar cells using hydrophobic antireflective inverted moth-eye nanopatterned PDMS films [J]. Advanced Energy Materials, 2014, 4(8): 1301315.
- [77] Wang W, Liu Y Q, Liu Y, et al. Direct laser writing of superhydrophobic PDMS elastomers for controllable

- manipulation via Marangoni effect [J]. Advanced Functional Materials, 2017, 27(44): 1702946.
- [78] Zhang Y L, Ma J N, Liu S, et al. A “Yin”-“Yang” complementarity strategy for design and fabrication of dual-responsive bimorph actuators [J]. Nano Energy, 2020, 68: 104302.
- [79] Zhang Y L, Liu Y Q, Han D D, et al. Quantum-confined-superfluidics-enabled moisture actuation based on unilaterally structured graphene oxide papers [J]. Advanced Materials, 2019, 31 (32): e1901585.
- [80] Han D D, Liu Y Q, Ma J N, et al. Biomimetic graphene actuators enabled by multiresponse graphene oxide paper with pretailored reduction gradient [J]. Advanced Materials Technologies, 2018, 3(12): 1800258.
- [81] Han D D, Zhang Y L, Ma J N, et al. Sunlight-reduced graphene oxides as sensitive moisture sensors for smart device design [J]. Advanced Materials Technologies, 2017, 2(8): 1700045.
- [82] Han D D, Zhang Y L, Ma J N, et al. Light-mediated manufacture and manipulation of actuators [J]. Advanced Materials, 2016, 28(38): 8328-8343.
- [83] Han D D, Zhang Y L, Liu Y, et al. Bioinspired graphene actuators prepared by unilateral UV irradiation of graphene oxide papers [J]. Advanced Functional Materials, 2015, 25(28): 4548-4557.
- [84] Han D D, Zhang Y L, Jiang H B, et al. Moisture-responsive graphene paper prepared by self-controlled photoreduction [J]. Advanced Materials, 2015, 27 (2): 332-338.
- [85] Müller-Meskamp L, Kim Y H, Roch T, et al. Efficiency enhancement of organic solar cells by fabricating periodic surface textures using direct laser interference patterning [J]. Advanced Materials, 2012, 24(7): 906-910.
- [86] Wang L, Xu B B, Chen Q D, et al. Maskless laser tailoring of conical pillar arrays for antireflective biomimetic surfaces [J]. Optics Letters, 2011, 36 (17): 3305-3307.
- [87] Li Q K, Cao J J, Yu Y H, et al. Fabrication of an anti-reflective microstructure on sapphire by femtosecond laser direct writing [J]. Optics Letters, 2017, 42(3): 543-546.
- [88] Zhang P P, Liao Q H, Yao H Z, et al. Three-dimensional water evaporation on a macroporous vertically aligned graphene pillar array under one Sun [J]. Journal of Materials Chemistry A, 2018, 6 (31): 15303-15309.
- [89] Ahn H J, Kim S I, Yoon J C, et al. Power conversion efficiency enhancement based on the bio-inspired hierarchical antireflection layer in dye sensitized solar cells [J]. Nanoscale, 2012, 4 (15): 4464.
- [90] Zhang X L, Song J F, Li X B, et al. Optical Tamm states enhanced broad-band absorption of organic solar cells [J]. Applied Physics Letters, 2012, 101(24): 243901.
- [91] Cho K S, Mandal P, Kim K, et al. Improved efficiency in GaAs solar cells by 1D and 2D nanopatterns fabricated by laser interference lithography [J]. Optics Communications, 2011, 284(10/11): 2608-2612.
- [92] Fang C L, Zheng J, Zhang Y J, et al. Antireflective paraboloidal microlens film for boosting power conversion efficiency of solar cells [J]. ACS Applied Materials & Interfaces, 2018, 10(26): 21950-21956.
- [93] Kang S B, Kim J H, Jeong M H, et al. Stretchable and colorless freestanding microwire arrays for transparent solar cells with flexibility [J]. Light: Science & Applications, 2019, 8: 121.
- [94] Kim J, Chhajed S, Schubert M, et al. Light-extraction enhancement of GaInN light-emitting diodes by graded-refractive-index indium tin oxide anti-reflection contact [J]. Advanced Materials, 2008, 20(4): 801-804.
- [95] Bai Y, Feng J, Liu Y F, et al. Outcoupling of trapped optical modes in organic light-emitting devices with one-step fabricated periodic corrugation by laser ablation [J]. Organic Electronics, 2011, 12 (11): 1927-1935.
- [96] Bi Y G, Feng J, Li Y F, et al. Broadband light extraction from white organic light-emitting devices by employing corrugated metallic electrodes with dual periodicity [J]. Advanced Materials, 2013, 25 (48): 6969-6974.
- [97] Li C H, Wang X P, Zhao J H, et al. Black silicon IR photodiode supersaturated with nitrogen by femtosecond laser irradiation [J]. IEEE Sensors Journal, 2018, 18(9): 3595-3601.
- [98] Li C H, Zhao J H, Chen Q D, et al. Sub-bandgap photo-response of non-doped black-silicon fabricated by nanosecond laser irradiation [J]. Optics Letters, 2018, 43(8): 1710-1713.
- [99] Guo C F, Sun T Y, Cao F, et al. Metallic nanostructures for light trapping in energy-harvesting devices [J]. Light: Science & Applications, 2014, 3 (4): e161.
- [100] Jalil S A, Lai B, ElKabbash M, et al. Spectral absorption control of femtosecond laser-treated metals and application in solar-thermal devices [J]. Light: Science & Applications, 2020, 9: 14.

- [101] Li J L, Wang X Y, Lin Z H, et al. Over 10 kg·m⁻²·h⁻¹ evaporation rate enabled by a 3D interconnected porous carbon foam[J]. Joule, 2020, 4(4): 928-937.
- [102] Li W G, Li Z, Bertelsmann K, et al. Portable low-pressure solar steaming-collection unisystem with polypyrrole origamis [J]. Advanced Materials, 2019, 31(29): e1900720.
- [103] Liu F H, Zhao B Y, Wu W P, et al. Low cost, robust, environmentally friendly geopolymers-mesoporous carbon composites for efficient solar powered steam generation[J]. Advanced Functional Materials, 2018, 28(47): 1803266.
- [104] Ren H Y, Tang M, Guan B L, et al. Hierarchical graphene foam for efficient omnidirectional solar-thermal energy conversion[J]. Advanced Materials, 2017, 29(38): e1702590.
- [105] He Z J, Xie X Z, Long J Y. Antireflective copper surfaces fabricated by low-cost nanosecond lasers for efficient photothermal conversion and desalination [J]. Journal of Laser Applications, 2019, 31(2): 022506.
- [106] Fan P X, Wu H, Zhong M L, et al. Large-scale cauliflower-shaped hierarchical copper nanostructures for efficient photothermal conversion [J]. Nanoscale, 2016, 8(30): 14617-14624.
- [107] Jiang G C, Pan R, Chen C H, et al. Ultrafast laser fabricated drag reduction micro-nano structures and their corrosion resistance [J]. Chinese Journal of Lasers, 2020, 47(8): 0802005.
江国琛, 潘瑞, 陈昶昊, 等. 超快激光制备水面减阻微纳结构及其耐蚀性研究[J]. 中国激光, 2020, 47(8): 0802005.
- [108] Lian Z, Xu J, Yu Z, et al. Bioinspired reversible switch between underwater superoleophobicity/superaerophobicity and oleophilicity/aerophilicity and improved antireflective property on the nanosecond laser-ablated superhydrophobic titanium surfaces[J]. ACS Applied Materials & Interfaces, 2020, 12(5): 6573-6580.
- [109] Wu D, Wang J N, Wu S Z, et al. Three-level biomimetic rice-leaf surfaces with controllable anisotropic sliding [J]. Advanced Functional Materials, 2011, 21(15): 2927-2932.
- [110] Wu D, Wu S Z, Chen Q D, et al. Facile creation of hierarchical PDMS microstructures with extreme underwater superoleophobicity for anti-oil application in microfluidic channels [J]. Lab on a Chip, 2011, 11(22): 3873-3879.
- [111] Zhou P Y, Peng Y Z, Huang Z M, et al. Fabrication and droplet impact performance of superhydrophobic surfaces developed using nanosecond lasers [J]. Chinese Journal of Lasers, 2020, 47(4): 0402012.
周培阳, 彭耀政, 黄泽铭, 等. 纳秒激光制备的超疏水表面及其液滴冲击性能[J]. 中国激光, 2020, 47(4): 0402012.
- [112] Zheng X G, Ding Y F, Wu H J. Surface wettability of aluminum alloy surface by laser etching after heat treatment [J]. Laser & Optoelectronics Progress, 2020, 57(15): 151406.
郑晓光, 丁云飞, 吴会军. 热处理后激光刻蚀铝合金表面润湿性的研究[J]. 激光与光电子学进展, 2020, 57(15): 151406.
- [113] Zhang Z B, Hua Y Q, Ye Y X, et al. Fabrication of superhydrophobic nickel-aluminum bronze alloy surfaces based on picosecond laser pulses [J]. Chinese Journal of Lasers, 2019, 46(3): 0302013.
章泽斌, 花银群, 叶云霞, 等. 基于皮秒激光的超疏水镍铝青铜合金表面的制备[J]. 中国激光, 2019, 46(3): 0302013.
- [114] Mao Z W, Cao W, Hu J, et al. A dual-functional surface with hierarchical micro/nanostructure arrays for self-cleaning and antireflection [J]. RSC Advances, 2017, 7(78): 49649-49654.
- [115] Domke M, Sonderegger G, Kostal E, et al. Transparent laser-structured glasses with superhydrophilic properties for anti-fogging applications [J]. Applied Physics A, 2019, 125(10): 675.
- [116] Li J, Zhou Y J, Wang W B, et al. Superhydrophobic copper surface textured by laser for delayed icing phenomenon[J]. Langmuir, 2020, 36(5): 1075-1082.

Research Progress on Laser Processing of Antireflection Surfaces

Jiao Zhizhen, Li Jichao, Chen Zhaodi, Han Dongdong, Zhang Yonglai *

State Key Laboratory of Integrated Optoelectronics, College of Electronic Science and Engineering, Jilin University, Changchun, Jilin 130012, China

Abstract

Significance The interaction between light and matter makes our world colorful, which includes absorption, reflection, scattering, transmission, diffraction, and interference. The antireflection (AR) characteristics of material surfaces are beneficial to improve the coupling of specific incident electromagnetic waves and the ability to distinguish particular electromagnetic signals. The AR characteristics are also helpful to shield and eliminate specific interference signals. Reducing the incident light reflection on material surfaces and improving reflection and transmission are vital to the utilization of solar energy, flat panel displays, infrared imaging, surface Raman enhancement, optoelectronic devices, military stealth, and aerospace technologies. Therefore, it is crucial to perform an effective light management and improve the performance of optical devices.

There exist many AR surface (ARS) fabrication methods, such as sol-gel, chemical vapor deposition, nanoimprinting, wet etching, dry etching, and laser processing. Among them, laser processing has attracted much attention owing to its advantages of high efficiency, programmability, high processing resolution, noncontact processing, high flexibility, and environment-friendly operation. Moreover, it is suitable for almost all materials (e.g., silicon-based materials, polymers, metal films, and carbon-based materials). Furthermore, femtosecond laser processing is a cold working process, which is highly suitable for complex and precise surface structure processing. Therefore, laser processing technologies stand out in the field of ARS preparation. To further improve the processing efficiency, multibeam parallel processing, or laser processing technology combined with other preparation methods such as wet etching or dry etching can be used. Above all, laser processing is a powerful tool for preparing AR structures on any material surfaces.

This review summarizes the latest progress in laser processing of ARSs, elaborates on the principle of AR and the selection of AR materials, and summarizes the current applications of ARSs in various fields, including solar cells, LEDs/OLEDs, photodetectors, and solar-driven water evaporators. Many excellent reports have described the preparation of ARSs; however, there are still some challenges in their large-scale industrial production and practical application. Therefore, summarizing the existing research is crucial to guide the future development of laser processing technologies.

Progress First, we summarize the principles of AR in detail using the Fresnel equation and elaborate on various structure sizes and light effects (Fig. 1). Then, according to previous reports, we summarize the advantages and disadvantages of various ARS preparation methods, structures and morphologies, and the scope of laser processing technologies (Table 1). In addition, we introduce how to effectively improve the efficiency of laser processing for preparing ARSs. For silicon-and silicon-oxide-based materials, Papadopoulos's research group has used circularly polarized ultrashort laser pulses to induce a subwavelength nanopillar structure on fused quartz, realizing a useful ARS with a full angle and broad spectral range (Fig. 2). For metal-based materials, Fan's research group has successfully prepared an AR micro-nano-hybrid structure on a copper surface using a laser direct writing strategy controlled by pulse injection (Fig. 3). For polymer matrices, Leem's research group has prepared a polydimethylsiloxane (PDMS) AR layer using a moth-eye AR structure on a glass substrate using double-beam interference combined with dry etching and transfer technology (Fig. 4). Moreover, silicon and silicon oxide, metals, and polymer-based materials are summarized comprehensively (Table 2). ARS applications such as solar cells (Fig. 5), OLEDs (Fig. 6), photodetectors (Fig. 7), solar-driven water evaporators (Fig. 8), and multifunctional bionic surfaces are discussed in detail. Finally, the existing problems in ARS preparation are discussed, with a focus on the processing efficiency, problems in practical applications, and the challenges in industrial production.

Conclusion and Prospect ARSs based on micro-nanostructures display excellent characteristics such as wide angle, broad spectra, and polarization insensitivity, and have been widely used in solar cells, LEDs/OLEDs, photodetectors, and photothermal conversion. As the ARS preparation technology continues to develop, laser

processing stands out owing to its high processing resolution, high efficiency, and programmable design. This review introduces the ARS technologies, including surfaces and morphologies, selection of AR materials, and the applications of ARSs, especially the progress in recent years. Although there are still some unresolved problems in the preparation of ARSs by laser processing, we firmly believe that through further in-depth research and structural optimization of existing ARSs, a much higher-quality ARS can be prepared. We expect these advances will bring development to many areas such as the photovoltaic industry, military, and aerospace industry as well as LEDs, and thus promote the development of renewable energy and national economy.

Key words laser technique; anti-reflection; laser processing; micro-nano structure; theory

OCIS codes 140.3390; 310.1210; 310.6628; 050.6624; 320.7160